Integrated Allosteric Model of Voltage Gating of HCN Channels

Claudia Altomare, Annalisa Bucchi, Eva Camatini, Mirko Baruscotti, Carlo Viscomi, Anna Moroni, and Dario DiFrancesco

From the Dipartimento di Fisiologia e Biochimica Generali, via Celoria 26, and INFM-Unità Milano Università, via Celoria 16, 20133 Milano, Italy

ABSTRACT Hyperpolarization-activated (pacemaker) channels are dually gated by negative voltage and intracellular cAMP. Kinetics of native cardiac f-channels are not compatible with HH gating, and require closed/open multistate models. We verified that members of the HCN channel family (mHCN1, hHCN2, hHCN4) also have properties not complying with HH gating, such as sigmoidal activation and deactivation, activation deviating from fixed power of an exponential, removal of activation "delay" by preconditioning hyperpolarization. Previous work on native channels has indicated that the shifting action of cAMP on the open probability (Po) curve can be accounted for by an allosteric model, whereby cAMP binds more favorably to open than closed channels. We therefore asked whether not only cAMP-dependent, but also voltage-dependent gating of hyperpolarization-activated channels could be explained by an allosteric model. We hypothesized that HCN channels are tetramers and that each subunit comprises a voltage sensor moving between "reluctant" and "willing" states, whereas voltage sensors are independently gated by voltage, channel closed/open transitions occur allosterically. These hypotheses led to a multistate scheme comprising five open and five closed channel states. We estimated model rate constants by fitting first activation delay curves and single exponential time constant curves, and then individual activation/deactivation traces. By simply using different sets of rate constants, the model accounts for qualitative and quantitative aspects of voltage gating of all three HCN isoforms investigated, and allows an interpretation of the different kinetic properties of different isoforms. For example, faster kinetics of HCN1 relative to HCN2/HCN4 are attributable to higher HCN1 voltage sensors' rates and looser voltage-independent interactions between subunits in closed/open transitions. It also accounts for experimental evidence that reduction of sensors' positive charge leads to negative voltage shifts of Po curve, with little change of curve slope. HCN voltage gating thus involves two processes: voltage sensor gating and allosteric opening/closing.

KEY WORDS: HCN channels • pacemaker • hyperpolarization-activated channels • modeling • channel gating

INTRODUCTION

Hyperpolarization-activated f/h channels, also referred to as "pacemaker" channels, have been described in a variety of cell types including cardiac and neuronal cells (DiFrancesco, 1985, 1993; Pape, 1996). In cells where pacemaker channels are expressed, their properties serve different purposes, normally associated to the ability to generate a depolarization upon activation by previous hyperpolarization or by the second messenger cAMP.

Four isoforms of hyperpolarization-activated, cyclic nucleotide–gated (HCN)[1] channels have been recently cloned in several organisms (Santoro et al., 1997, 1998; Gauss et al., 1998; Ludwig et al., 1998, 1999; Seifert et al., 1999; Vaccari et al. 1999). Expression experiments have demonstrated that HCN channels are the cloned equivalents of native f/h channels (Santoro et al., 1998; Ishii et al., 1999; Ludwig et al., 1999; Seifert et al., 1999; Moroni et al., 2000). HCN sequences are homologous to those of Kv and cyclic nucleotide–gated (CNG) channels (Clapham, 1998), and belong to the same superfamily of six transmembrane (TM) domain channels.

The availability of different isoforms of HCN channels allows a detailed analysis of isoform-specific gating and modulatory properties, and a comparison of these properties with those of native channels as a way to corroborate expression data. Further, the existence of HCN isoforms with different gating properties prompts the question whether a comprehensive model can be developed to describe the kinetic features of the HCN family.

In this work we have analyzed detailed properties of voltage gating of three HCN clones (mHCN1, hHCN2, and hHCN4) based on the following considerations. First, it is known that kinetic features of native f-channel activation/deactivation cannot be described satisfactorily by the use of Hodgkin-Huxley (HH) description (DiFrancesco, 1984). To account for these features, a complex kinetic model based on the coexistence of a "delaying" and a proper "gating" process and involving five voltage-dependent gating variables of three dif-

Address correspondence to Dario DiFrancesco, Università di Milano, Dipartimento di Fisiologia e Biochimica Generali, via Celoria 26, 20133 Milano, Italy. Fax: 39-02-70632-884. E-mail: dario.difrancesco@unimi.it

[1]*Abbreviations used in this paper:* CNG, cyclic nucleotide–gated; HCN, hyperpolarization-activated, cyclic nucleotide–gated; HH, Hodgkin-Huxley; MWC, Monod-Whyman-Changeaux; Po, open probability; SAN, sinoatrial node; TM, transmembrane.

ferent types had been previously proposed (DiFrancesco, 1984). Second, voltage gating of several ion channels has been recently interpreted on the basis of allosteric models (Marks and Jones, 1992; Rìos et al., 1993; McCormack et al., 1994; Horrigan and Aldrich, 1999; Horrigan et al., 1999; Jones, 1999). Third, the structural homology of HCN channels to 6-TM domain K^+ channels favors the hypothesis that HCN channels, too, are tetramers.

Our starting point was based on a recent investigation in cardiac SAN cells, showing that basic kinetic and modulatory properties of native pacemaker f-channels can be explained by a hybrid HH-MWC model (DiFrancesco, 1999). In that model, voltage gating was described by a standard HH scheme with two independent subunits, while cAMP-induced activation occurred according to a cyclic allosteric Monod-Wyman-Changeaux (MWC) model (Monod et al., 1965) involving binding of one cAMP molecule per gating subunit.

On the basis of the above considerations, we explored the possibility that, as well as by cAMP, gating of pacemaker channels is modulated allosterically by voltage, too. In this attempt, we extended the hypothesis made in the gating scheme proposed earlier (DiFrancesco, 1999) that pacemaker channels are composed of subunits, each independently gated by voltage and cAMP. We made the assumption that, like *mSlo* channels (Horrigan and Aldrich, 1999; Horrigan et al., 1999), HCN channels are homotetramers, with each subunit carrying one independent voltage sensor, and that closed/open channel transitions involve concerted structural modifications of all four subunits and occur allosterically.

We found that by simply selecting an appropriate set of rate constants for each isoform, the allosteric assumption accounts for quantitative features of voltage-dependent gating of different isoforms. The allosteric hypothesis provides an interpretation of the possible mechanisms responsible for the different gating properties of different isoforms, and may represent an unifying model for HCN channel gating.

MATERIALS AND METHODS

Molecular Biology

Functional Expression of HCN Clones in Phoenix Cells

Mouse HCN1 cDNA (mHCN1) (construct pSD64TF, provided by Dr. B. Santoro, Columbia University, New York), was cut with EcoRV and NotI restriction enzymes, filled blunt and ligated into the eukaryotic expression vector pIRES-EGFP (CLONTECH Laboratories, Inc.) predigested with EcoRV. Human HCN2 minigene (hHCN2) was subcloned into the eukaryotic expression vector pcDNA3.1 (Invitrogen) as previously described (Vaccari et al., 1999). Human HCN4 (hHCN4) was provided by Dr. U.B. Kaupp (Forschungszentrum, Jülich, Germany) in the eukaryotic expression vector pcDNA1 (CLONTECH Laboratories, Inc.). For transient functional expression channel-specific cDNA was transfected into modified HEK 293 (Phoenix) cells (Kinsella and Nolan 1996; Moroni et al., 2000). hHCN2 and hHCN4 constructs were cotransfected with a GFP-containing plasmid. In brief, for each 35-mm Petri dish we used 7 μg of channel-specific construct and 3.5 μg of GFP-containing plasmid. In the case of mHCN1/pIRES-EGFP, we used 10 μg of construct, which coexpresses the channel and the GFP protein on a polycystronic mRNA. Phoenix cells were cultured in Dulbecco's modified essential medium supplemented with 10% FCS (GIBCO BRL) and antibiotics (Sigma-Aldrich). In the following text, the species symbol will be dropped for simplicity and the mHCN1, hHCN2, hHCN4 isoforms will be termed HCN1, HCN2, and HCN4, respectively.

Electrophysiology

Experiments were performed on Phoenix cells incubated after transfection at 37°C in 5% CO_2 for 1– 5 d. Before electrophysiological measurements, cells were dispersed by trypsinization and plated onto 35-mm plastic Petri dishes at low density, where they were allowed to settle for 3–4 h. Petri dishes were transferred under the stage of an inverted microscope, and single cells were patch-clamped in the whole-cell configuration according to standard methods (Moroni et al., 2000). For the analysis, we visually selected strongly GFP-reactive cells. Cells were perfused at room temperature (24–25°C) with a control Tyrode solution containing (in mM): 140 NaCl, 5.4 KCl, 1.8 $CaCl_2$, 1 $MgCl_2$, 5.5 D-glucose, and 5 HEPES-NaOH, pH 7.4. The solution was delivered via a fast-flow perfusion pipet.

Whole-cell pipets were filled with an intracellular-like solution containing (in mM): 10 NaCl, 130 KCl, 1.0 EGTA, 5 HEPES-KOH, 0.5 $MgCl_2$, 2 ATP (sodium salt), 0.1 GTP (sodium salt), and 5 phosphocreatine, pH 7.2. We added 1 mM $BaCl_2$, 2 mM $MnCl_2$, 100 μM $NiCl_2$, and 20 μM nifedipine to perfusing solutions (in mM: 110 NaCl, 30 KCl, 1.8 $CaCl_2$, 0.5 $MgCl_2$, and 5 HEPES-NaOH, pH 7.4) to reduce interference from overlapping Ca^{2+} and K^+ components in the measurement of HCN currents.

Data Analysis

Activation curves were obtained by standard two-step voltage-clamp protocols previously used (DiFrancesco et al., 1986; Moroni et al., 2000). The protocols consisted of hyperpolarizations applied in 10-mV steps from a fixed holding potential of −35 mV, followed by steps to test voltages where the amplitude of deactivation current tails was measured. The duration of activation steps varied with the test voltage to allow attainment of steady-state.

Curve Fitting

For all HCN isoforms investigated, activation/deactivation traces were fitted by single exponential curves after an initial delay; delay, time-constant, and current amplitude were free to vary in the best-fitting routine.

Numerical Computations

Analytical treatment of the allosteric scheme proposed (see Fig. 2) is given in the APPENDIX. Calculations were performed by integration of the vectorial differential equation (A2):

$$\frac{dp}{dt} = A \cdot p + k,$$

where the probability vector p, the vector k, and the matrix A are defined in the APPENDIX. The integration was performed by a fourth order Runge-Kutta approximation method, with an integration step set to 1/1,500th of the total integration time. The channel open probability at any time t was calculated as Po(t) =

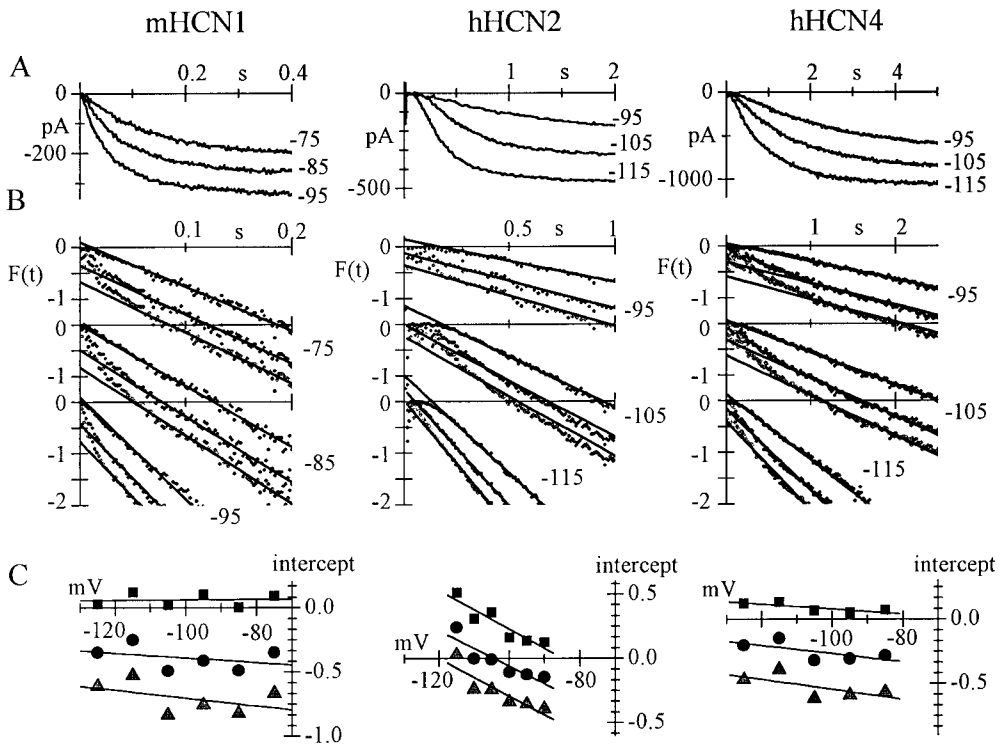

FIGURE 1. Activation kinetics of HCN isoforms are not compatible with a fixed power of an exponential. (A) Sample current traces recorded on hyperpolarization to the voltages indicated from a holding potential of −35 mV in Phoenix cells expressing HCN1 (left), HCN2 (middle), and HCN4 (right). Voltage steps were long enough to reach steady state for each trace, and only a fraction of the records is shown on an expanded time scale to highlight the time course at early times. (B) Plots of the function $F(t) = \ln(1 - (I(t)/I_\infty)^{1/n})$, where I is current and I_∞ the steady-state current value for traces in A, at the voltages indicated. For each voltage, the function F(t) was plotted for values of n = 1, 2, and 3 (top to bottom trace) and the linear part fitted by straight lines (full lines). Traces at different voltages are shifted vertically for clarity. If activation occurs according to the nth power of an exponential of time constant τ, then $F(t) = -t/\tau$ and F(t) plots should be straight lines with zero y-intercept. (C) Values of vertical intercepts at t = 0 of linear fittings of F(t) plots in B, plotted against voltage for n = 1 (squares), n = 2 (circles) and n = 3 (triangles). These values represent "delays" (if positive) or "anticipations" (if negative) relative to a time course developing according to the selected power of exponential.

$p_6(t) + p_7(t) + p_8(t) + p_9(t) + p_{10}(t)$. In computations reproducing experimental current kinetics, the predicted current time course at a given voltage V was calculated as $I(V,t) = I_{max}(V) \cdot Po(V,t)$, where $I_{max}(V) = g_{max} \cdot (V - V_{rev})$ was the fully activated current extrapolated from experimental data.

To reproduce individual experimental traces (Figs. 4–6) we used a semi-empirical fitting routine. Computations were initially performed by assigning first-guess values to the selected parameters, chosen by previous identification of general criteria for restricting parameter values (see RESULTS) and then by trial-and-error approximation, until satisfactory simulations were obtained.

RESULTS

HCN Channels Have Kinetic Properties That Are Not Compatible with HH Models

Early investigation of the kinetics of native hyperpolarization-activated channels (f-channels of cardiac Purkinje fibres) has identified features that are not compatible with HH gating models. These include a sigmoidal activation time course that cannot be described by a fixed power of an exponential at all voltages, sigmoidal deactivation and removal of activation "delay" by conditioning prehyperpolarizing steps (DiFrancesco, 1984).

To probe whether HCN channels also have features not complying with HH kinetics, we analyzed the time course of current activation in cells expressing HCN1, HCN2, or HCN4, and checked if it could be described by a fixed power of an exponential. In Fig. 1 A, HCN1, HCN2, and HCN4 current activation traces recorded on hyperpolarization at voltages in the range −75 to −115 mV are shown. Plots of the function $F(t) = \ln(1 - (I(t)/I_\infty)^{1/n})$ should result in straight lines with zero y-intercepts and slope $= -1/\tau$ if the current activates according to the nth power of an exponential. To verify this, we plotted in Fig. 1 B the function F(t) for each current record with n = 1, 2 and 3, and in Fig. 1 C, we plotted the y-intercepts of fits to the linear part of F(t) plots.

Clearly, in none of the three examples presented can a fixed power of an exponential adequately describe the time course at all voltages. This is especially evident for HCN2. The voltage dependence is less marked for HCN4 and absent for HCN1, but a delay is apparent also for these two isoforms (see also Fig. 3). The analysis of Fig. 1 shows that, for all isoforms investigated, the activation time course can be described as a single exponential after a delay. The delay is small in HCN1, larger in HCN4 and most marked in HCN2 records.

Other gating properties of native f-channels in Purkinje fibres that cannot be reconciled with HH kinetics include sigmoidal deactivation and the removal of activation delay by conditioning prehyperpolarizing steps (DiFrancesco, 1984). Both these features are also observed in HCN channels, and are dealt with later (Figs. 4–6 and 8). These observations indicate that, as in native f-channels, voltage gating of HCN channels is not compatible

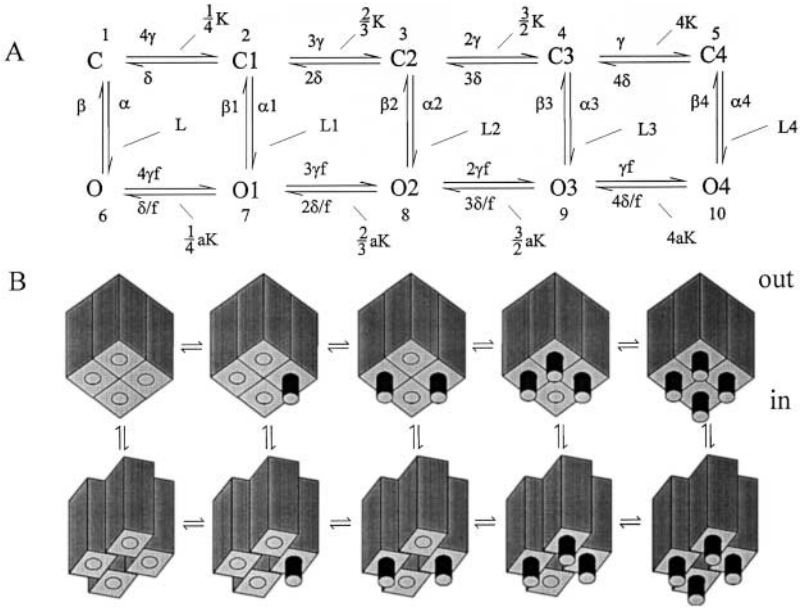

FIGURE 2. Proposed allosteric scheme of voltage gating of HCN channels. (A) Reaction scheme. (B) Physical model; only one of the possible configurations with 1, 2, or 3 willing sensors are shown. The channel is assumed to be composed of four identical subunits, each carrying one voltage sensor (round bars in B) that can assume two different configurations: one "reluctant" (hidden) and one willing (protruding from the subunit) to help the opening process. Closed/open transitions occur allosterically and involve concerted structural modifications of all four subunits. This results in 10 different states, 5 closed (C–C4) and 5 open (O–O4). Labels 1–4 identify the number of voltage sensors in the willing position (zero unlabeled). States are numbered 1–10 (in A) to allow matrix identification of rate constants (see APPENDIX). Voltage sensors act independently of the subunit to which they belong. Each rate constant is multiplied by the number of possible transitions. To reproduce hyperpolarization-induced activation, the model assumes a voltage dependence of rate constants favoring left-to-right and top-to-bottom transitions upon hyperpolarization, which according to the Boltzmann equation (Eq. A9 of APPENDIX) describing α, β, γ, and δ implies $z_\alpha < 0$, $z_\beta > 0$, $z_\gamma < 0$, and $z_\delta > 0$. Transition of any one voltage sensor to the willing state is assumed to increase the probability of channel opening. This is achieved by multiplying closed/open equilibrium constants by a constant value ($a < 1$) any time one sensor moves to the willing position (L to L1, L1 to L2, etc.). Assuming "balanced" rate constant changes, this implies that opening rate constants are divided by $\sqrt{a}$ (α to α1, α1 to α2, etc.), and closing rate constants are multiplied by $\sqrt{a}$ (β to β1, β1 to β2, etc.). Because of the cyclic arrangement, similar relations hold for reluctant/willing equilibrium constants and rate constants when channels switch from closed to open. Defining $f = 1/\sqrt{a}$, the following relations thus hold (see Eq. A6):

$$K = \frac{4[C]}{[C1]} = \frac{3[C1]}{2[C2]} = \frac{2[C2]}{3[C3]} = \frac{[C3]}{4[C4]} = \frac{\delta}{\gamma};$$

$$aK = \frac{\delta/f}{\gamma f} = \frac{K}{f^2}$$

$$L = \frac{[C]}{[O]} = \frac{\beta}{\alpha}; \qquad Li = \frac{[Ci]}{[Oi]} = \frac{\beta i}{\alpha i} = a^i L \qquad (i = 1\text{–}4)$$

$$\alpha i = \alpha f^i; \qquad \beta i = \frac{\beta i}{f^i} \qquad (i = 1\text{–}4)$$

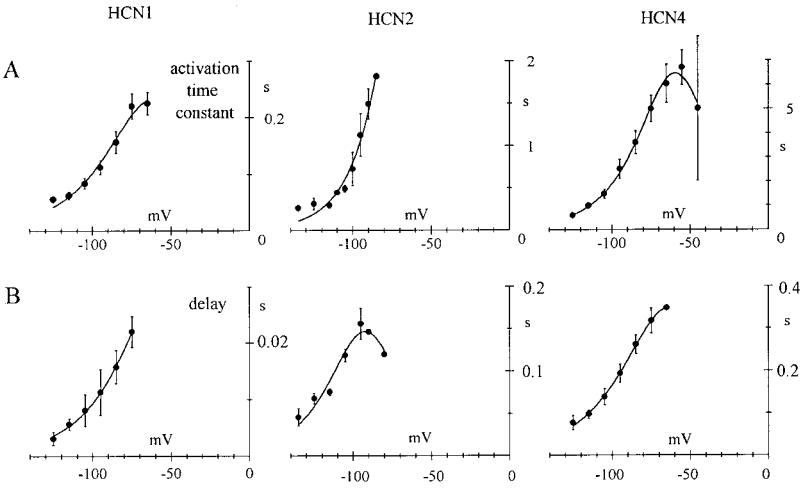

FIGURE 3. (A) Voltage dependence of time constants (mean ± SEM) measured by fitting activation current traces by single exponentials after an initial delay for HCN1 (left, $n = 9$), HCN2 (middle, $n = 7$), and HCN4 channels (right, $n = 13$). Data points were fitted with the equation $\tau 4L(V) = 1/(\alpha 4(V) + \beta 4(V)) = 1/(\alpha(V)/a^2 + \beta(V)a^2))$, with $a = 0.2$ and $\alpha(V)$ and $\beta(V)$ as in Eq. A9, which yielded the following parameters: for HCN1, $\alpha o = 0.008716\ s^{-1}$, $\beta o = 522.6\ s^{-1}$, and $z_\beta (= -z_\alpha) = 0.9674$; for HCN2, $\alpha o = 0.0001712\ s^{-1}$, $\beta o = 26.17\ s^{-1}$, and $z_\beta (= -z_\alpha) = 1.465$; and for HCN4, $\alpha o = 0.0001912\ s^{-1}$, $\beta o = 31.27\ s^{-1}$, and $z_\beta = (-z_\alpha) = 1.211$. (B) Voltage dependence of the delay preceding single exponential time course of currents (mean ± SEM) during hyperpolarization for HCN1 (left, $n = 9$), HCN2 (middle, $n = 5$) and HCN4 channels (right, $n = 10$). Data points were fitted with the equation $\tau K(V) = 1/(\delta(V) + \gamma(V))$, with $\delta(V)$ and $\gamma(V)$ as in Eq. A9, which yielded the following parameters: for HCN1, $\gamma o = 2.296\ s^{-1}$, $\delta o = 95.14\ s^{-1}$, and $z_\delta (= -z_\gamma) = 0.9853$; for HCN2, $\gamma o = 0.04025\ s^{-1}$, $\delta o = 287.5\ s^{-1}$,and $z_\delta (= -z_\gamma) = 1.242$; and for HCN4, $\gamma o = 0.1387\ s^{-1}$, $\delta o = 14.78\ s^{-1}$, and $z_\delta (= -z_\gamma) = 0.9577$. All values of best-fitting parameters are reported in Table I.

with HH models, and require more complex gating schemes involving multiple open and closed states.

Description of Kinetic Properties of HCN Channels by Allosteric Voltage-dependent Gating

In Fig. 2, the reaction scheme used to describe allosteric voltage-dependent gating of HCN channels is shown. Channels are thought to be composed of four subunits, each possessing one voltage sensor that can assume two configurations (one "willing" and one "reluctant" to open channels) and that is gated independently by voltage. With the allosteric hypothesis, all subunits undergo simultaneous, concerted transitions between closed/open states.

The analytical treatment, and the methods for numerical computations of the kinetics predicted by the model in Fig. 2 are described in APPENDIX. Under the assumptions made, the kinetic behavior of the allosteric model is fully characterized by knowledge of the parameter a and the eight parameters αo, βo, γo, δo, z_α, z_β, z_γ, and z_δ describing the voltage dependence of rate constants α, β, γ, δ according to Eq. (A9). A further simplification is obtained by setting $z_\beta = -z_\alpha$, $z_\gamma = -z_\delta$ (see APPENDIX). This reduces the overall free parameters to $n = 7$.

HCN Channels Activation and Deactivation Kinetics: Selection of First-guess Fitting Parameters

Since the number of free parameters needed to simulate channel kinetics ($n = 7$) was too large to allow adequate fitting of data, we searched for criteria to restrict parameters values. The parameter "a" represents the multiplying factor of equilibrium constants of closed/open transitions upon movement of one voltage sensor from the reluctant to the willing state.

The model assumes that the transition of a voltage sensor to the willing state increases the open-to-closed channel ratio by a fixed factor, regardless of the channel subunit the voltage sensor belongs to. This implies that the parameter a is a constant in the range $0 < a < 1$. Values of "a" close to 1 determine the condition $L \approx L1 \approx L2 \approx L3 \approx L4$, corresponding to practically ineffective voltage sensors; this would tend to abolish delays in activation and deactivation. Small values of "a" ($a \ll 1$), on the other hand, determine the condition $L \gg L1 \gg L2 \gg L3 \gg L4$. This would imply that most openings occur when all four voltage sensors are in the willing state (C4 $\rightarrow$O4), and that activation kinetics could be approximated by the linear scheme C$\rightarrow$C1$\rightarrow$C2$\rightarrow$C3$\rightarrow$C4$\rightarrow$O4, with well separated "delaying" (C$\rightarrow$C4) and "opening" (C4$\rightarrow$O4) processes. Because of the symmetry of the cyclic allosteric scheme proposed, small values of "a" would also favor closing to occur mainly when all voltage sensors are in the reluctant state (O$\rightarrow$C).

To test the predictive ability of the model, we tentatively assumed a = 0.2 and ran pilot computations. We found that, indeed, as expected for small values of a, the single exponential time course (after a delay) of computed activation traces approximated that of C4$\rightarrow$O4 transitions (time constant τ4L; see Eq. A10). We also noticed that plots of the delay displayed a voltage dependence similar to that of the time constant of voltage sensor transitions (τK(V); see Eq. A10), reflecting the fact that, in the model of Fig. 2, the process responsible for delaying channel opening is the displacement of voltage sensors from reluctant to willing states (data not shown).

These preliminary observations provided a method for a rough estimate of some of the required parameters. We fitted experimental traces by single exponentials after an initial delay. Plots of time constant and delay data, thus, measured for HCN1, HCN2, and HCN4 channels are shown in Fig. 3. We best-fitted the time constant data with the equation for τ4L(V) (see Eq. A10; Fig. 3 A); this yielded the functions α4(V) and β4(V), from which first-guess parameters αo, βo, and z_β ($= -z_\alpha$) could be calculated as reported in the legend to Fig. 3.

Delay data (Fig. 3 B) were also best-fitted with the equation for τK(V) (see Eq. A10); this generated the functions γ(V) and δ(V), from which the parameters γo, δo, and z_δ ($= -z_\gamma$) were calculated as reported in Fig. 3 legend. Table I lists the fitting parameters that were used as an initial set for predicting the kinetic behavior of the three HCN isoforms investigated.

To verify if the parameters in Table I could represent a starting set for subsequent fitting of kinetic data, we selected representative experimental current traces recorded during activation/deactivation voltage-clamp protocols, and used the parameter values in Table I to run model computations with the same protocols. We found that despite the elementary criteria used to select rate parameters, the computations appeared to succeed in reproducing qualitatively the main kinetic features of the three HCN isoforms, including the voltage dependence of rates of activation and deactivation and the different degrees of activation and deactivation delay for different isoforms, although, not surprisingly, they failed to reproduce accurately the time course of individual traces. To verify how the parameter a af-

TABLE I

First-guess Model Parameters

	αo	βo	γo	δo	$z_\beta = -z_\alpha$	$z_\delta = -z_\gamma$
HCN1	0.008716	522.6	2.296	95.14	0.9674	0.9853
HCN2	0.0001712	26.17	0.04025	287.5	1.465	1.242
HCN4	0.0001912	31.27	0.1387	14.78	1.211	0.9577

Parameters used for first approximation prediction of the kinetics of HCN channels by the allosteric model of Fig. 2, which was obtained by fitting of experimental data in Fig. 3. The parameter a was set to 0.2.

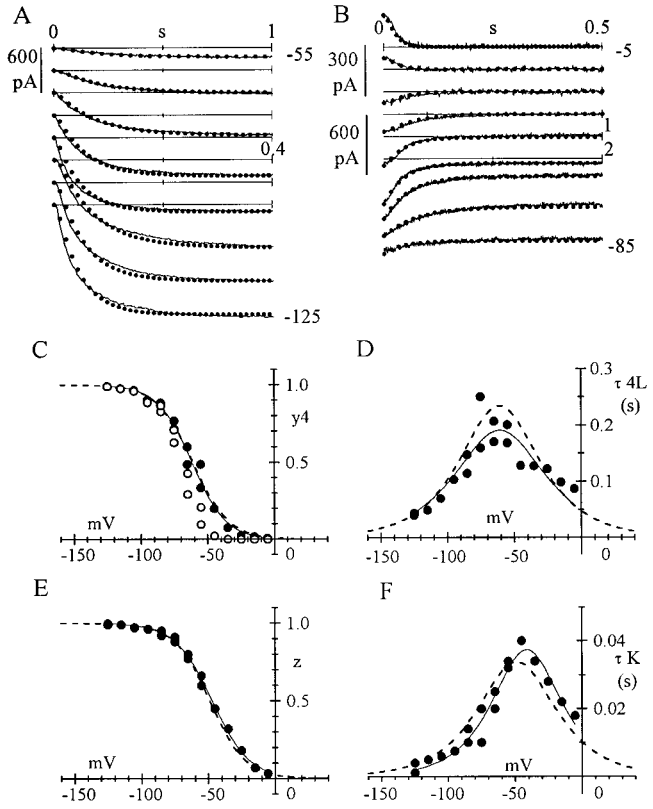

FIGURE 4. Simulation of activation and deactivation kinetics of HCN1 channel by allosteric model. Computations were carried out as outlined in the MATERIALS AND METHODS. (A) Activation traces recorded in a cell (lines) during steps from −35 mV to voltages in the range −55 to −125 mV (10-mV steps), as indicated, and corresponding computed traces (dots). Traces displaced vertically for clarity. (B) Deactivation traces recorded in the same cell (lines) during steps to the range −85 to −5 mV (10-mV steps), as indicated, preceded by a 1.2-s activation step to −125 mV from the holding potential of −35 mV, and corresponding computed traces (dots). The top three traces (−5, −15, and −25 mV) are plotted on a more expanded current scale. Traces at −55 to −85 mV are plotted on the same scale, and the remaining records are shifted vertically for clarity. (C and E) Plots of individual fractional activation values y4 (C) and z (E) (closed circles) used to fit individual experimental traces in A and B (for definition of y4 and z, see Eq. A10). Also plotted for comparison are the theoretical curves y4(V) and z(V) calculated with the rate constant parameters in Table I (broken lines) and the curves obtained by best-fitting of data points with the functions (Eq. A10; full lines). Best-fitting yielded the values: V4L= −61.71 mV; VK = −47.12 mV; z_β = 1.019; z_δ = 0.9310. Also plotted in C are open probability (Po) values obtained by the fitting parameters according to Eq. (A13) (open circles). (D and F) Plots of time constant values τ4L (D) and τK (F) (Eq. A10) used to fit experimental records in A and B, along with the theoretical curves τ4L(V) (D) and τK(V) (F) calculated from parameters in Table I (broken lines) and with best-fitting curves (full lines). Best-fitting yielded the following values: V4L = −60.74 mV; VK = −41.24 mV; z_β = 0.8551; z_δ = 1.105; α4o = 0.3515 s^{-1}; γo = 2.289 s^{-1}.

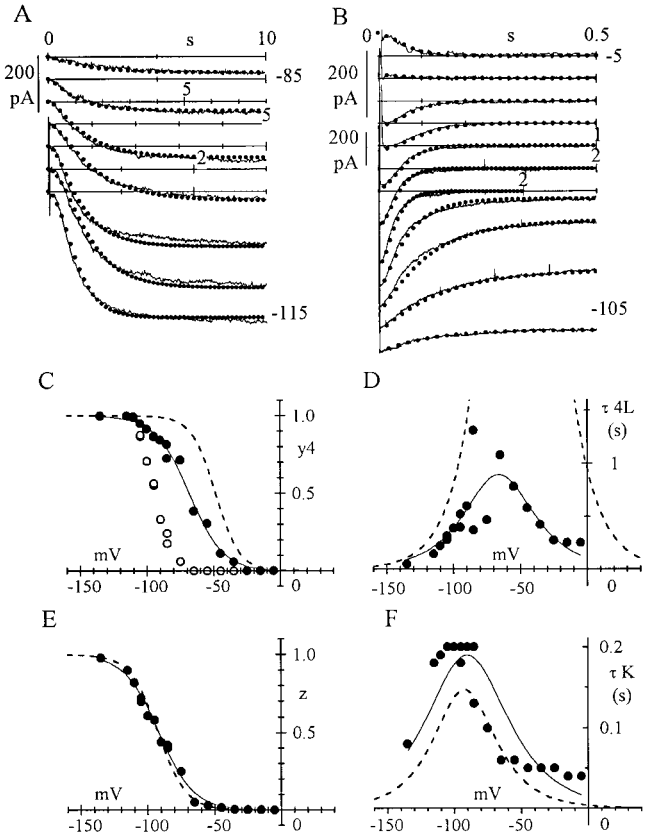

FIGURE 5. Simulation of activation and deactivation kinetics of HCN2 channel by allosteric model. Computations as in Fig. 4. (A) Activation traces recorded in a cell (lines) during steps from −35 mV to voltages in the range −85 to −115 mV (5-mV steps), as indicated, and corresponding computed traces (dots). Traces are displaced vertically for clarity. (B) Deactivation traces recorded in a different cell (lines) during steps to the range −5 to −105 mV (10-mV steps), as indicated, preceded by a 1-s activation step to −135 mV from the holding potential of −35 mV, and corresponding computed traces (dots). The top three traces (−5, −15, and −25 mV) are plotted on a more expanded current scale. Traces at −65 to −105 mV are plotted on the same scale, and the remaining records are shifted vertically for clarity. (C and E) Plots of fractional activation values y4 (C) and z (E) (closed circles) used to fit individual experimental traces in A and B (Eq. A10) and their best-fitting curves (full lines) along with the theoretical curves y4(V) and z(V) calculated with the parameters in Table I (broken lines). Best-fitting yielded the following values: V4L = −68.26 mV, VK = −91.61 mV, z_β = 1.023, and z_δ = 1.003. Also plotted in C are Po values obtained by the fitting parameters according to Eq. A13 (open circles). (D and F) Plots of time constant values τ4L (D) and τK (F) (Eq. A10) used to fit experimental records in A and B along with their best-fitting curves (full lines), and the theoretical curves τ4L(V) (D) and τK(V) (F) calculated from parameters in Table I (broken lines). Best-fitting yielded the following values: V4L = −66.05 mV,; VK = −101.5 mV, z_β = 1.110, z_δ = 1.040, α4o = 0.0327 s^{-1}, and γo = 0.04214 s^{-1}.

fected computed channel kinetics, prediction tests were also performed using a = 0.1, 0.3, and 0.5, and were less satisfactory (data not shown). Therefore, we selected a = 0.2.

Fitting of Activation and Deactivation Time Course for HCN1, HCN2, and HCN4 Channels

To verify if the model was able to more accurately mimic the kinetics of current activation and deactiva-

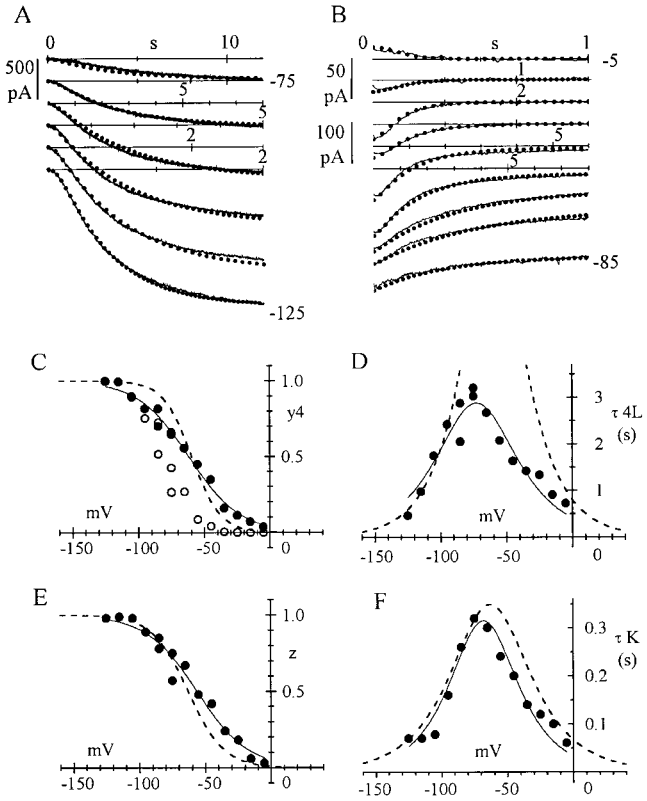

FIGURE 6. Simulation of activation and deactivation kinetics of HCN4 channel by allosteric model. Computations as in Fig. 4. (A) Activation traces recorded in a cell (lines) during steps from −35 mV to voltages in the range −75 to −125 mV (10-mV steps), as indicated, and corresponding computed traces (dots). Traces displaced vertically for clarity. (B) Deactivation traces recorded in a different cell (lines) during steps to the range −5 to −85 mV (10-mV steps), as indicated, preceded by a 2-s activation step to –125 mV from the holding potential of –35 mV, and corresponding computed traces (dots). The top three traces (−5, −15, and −25 mV) are plotted on a more expanded current scale. Traces at −55 to −85 mV are plotted on the same scale, and the remaining records are shifted vertically for clarity. (C and E) Plots of fractional activation values y4 (C) and z (E) (closed circles) used to fit individual experimental traces in A and B (Eq. A10) and their best-fitting curves (full lines) along with the theoretical curves y4(V) and z(V) calculated with the parameters in Table I (broken lines). Best-fitting yielded the following values: V4L = −61.66 mV; VK =−56.22 mV; z_β = 0.67; and z_δ = 0.6729. Also plotted in C are Po values obtained by the fitting parameters according to Eq. A13 (open circles). (D and F) Plots of time constant values τ4L (D) and τK (F) (Eq. A10) used to fit experimental records in A and B along with their best-fitting curves (full lines), and of the theoretical curves τ4L(V) (D) and τK(V) (F) calculated from parameters in Table I (broken lines). Best-fitting yielded the values: V4L = −72.68 mV; VK = −68.07 mV; z_β = 0.9384; z_δ = 1.114; α4o = 0.0124 s^{-1}; and γo = 0.08444 s^{-1}.

tion of HCN channels in specific cases, we used semi-empirical fitting routines on individual sets of traces as shown in Figs. 4–6 for HCN1, HCN2, and HCN4 channels, respectively.

For each trace, we initially used Table I to assign starting values to selected parameters (y4, z, τ4L, and τK) and calculated the rate constants α, β, γ, and δ according to Eqs. A10 and A6 of APPENDIX. These values (with a = 0.2) allowed calculation of the matrix A and of vector k (Eqs. A7b and A8), and thus of the current time course. The process was repeated by trial-and-error approximation, until a satisfactory simulation was obtained.

TABLE II

Fine-guess Model Parameters

	αo	βo	γo	δo	$z_\beta = -z_\alpha z_\delta = -z_\gamma$	
HCN1	0.01406	743.6	2.289	74.36	0.9369	1.018
HCN2	0.001308	208.4	0.04214	86.66	1.066	1.021
HCN4	0.000496	20.25	0.08444	6.196	0.8042	0.8934

Allosteric model parameters deduced by best-fitting of kinetic parameters of HCN channels. As reported in Figs. 5–7, pairs of values z_β,z_δ, V4L, and VK for HCN1, HCN2, and HCN4 were obtained by best-fitting probability distribution curves (y4(V) and z(V)) or time constant curves (τ4L(V) and τK(V)). Fitting of time constant curves also yielded values for α4o and γo. After averaging the pairs of values of V4L, VK, z_β and z_δ, we calculated αo as αo = α4oa^2 and βo and γo according to Eqs. A15 and A17.

For all isoforms, the model was able to reproduce the detailed kinetic features of activation and deactivation in the whole voltage range investigated. The data points selected with the above procedure for y4, z, τ4L, and τK deviated from the first-guess values assumed on the basis of the preliminary analysis of Fig. 3 (compare closed circles with broken lines in Figs. 4–6, panels C–F). They were best-fitted using the equations for y4, z, τ4L, and τK (see Eqs. A6, A9, and A10) and the resulting rate parameters are reported in Table II. These can be directly compared with those of Table I.

Steady-state Open Probability

Steady-state solution of the allosteric model in Fig. 2 yields the open probability-voltage relation Po(V) expressed by Eq. (A13), which clearly does not represent a Boltzmann type of voltage dependence. Nonetheless, to verify if it can describe the steady-state open probability curve of HCN channels, we used it to fit in Fig. 7 the mean activation curves for HCN1, HCN2, and HCN4.

For all three isoforms, the allosteric Po relation was able to fit adequately the steady-state activation curves. Po values obtained independently by fitting activation/deactivation kinetics in Figs. 4–6 (open circles) fell near the Po curves (full lines) obtained with Eq. A13, indicating that the two procedures led to comparable predictions.

Removal of the Delay in Current Activation by Conditioning Prehyperpolarization

In cardiac Purkinje fibres, activation delay can be removed by conditioning prehyperpolarizations (DiFrancesco, 1984). To verify whether HCN channels have the same property, we applied two-step protocols to cells expressing HCN4 channels. As apparent in the example of Fig. 8 A, short prehyperpolarizations to

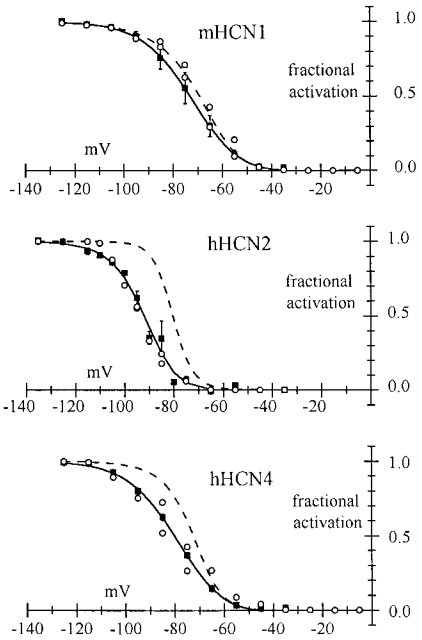

FIGURE 7. Fitting of activation curves for HCN1, HCN2 and HCN4. Activation curves were measured as explained in MATERIALS AND METHODS in cells expressing HCN1 ($n = 8$), HCN2 ($n = 3$) and HCN4 channels ($n = 11$). Data points (closed squares) are plotted as mean ± SEM values. The curves were fitted with Eq. A13:

$$P(o) = \frac{1}{1 + L(V)\left(\frac{1 + 1/K(V)}{1 + 1/aK(V)}\right)^4},$$

where the voltage dependence of L and K is described by Eqs. A14 and A15. In the fitting procedure, initial values of the parameters were those reported in Table I (broken lines). Best-fitting yielded the following parameters: for HCN1 (top), $z_\beta = 1.212$, $z_\delta = 1.150$, VL = −140.6 mV (V4L = −71.94 mV), and VK = −34.4 mV; for HCN2 (middle), $z_\beta = 1.501$, $z_\delta = 1.032$, VL = −143.3 mV (V4L = −87.86 mV), and VK = −68.9 mV; and for HCN4 (bottom), $z_\beta = 1.255$, $z_\delta = 1.540$, VL = −145.9 mV (V4L = −79.60 mV), and VK = −46.1 mV. V4L values were calculated according to Eq. A17. Also plotted for comparison (open circles) are Po values obtained from the kinetic analysis of Figs. 4– 6.

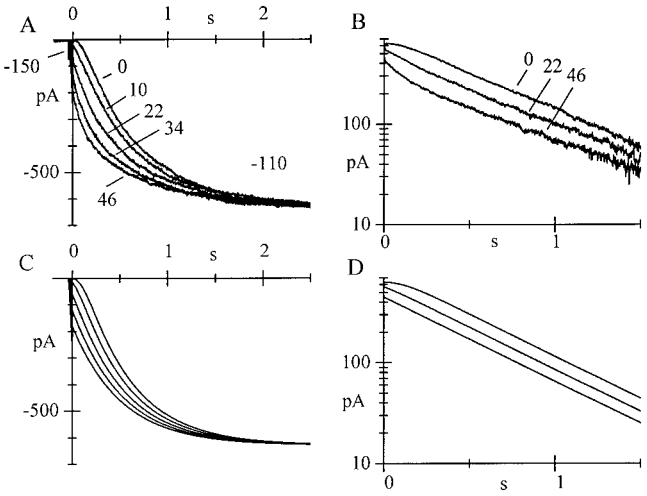

FIGURE 8. Removal of activation delay by prehyperpolarization and prediction of allosteric model. (A) Current traces recorded from a cell expressing HCN4 channels during 3-s steps to −110 mV after prehyperpolarizations to −150 mV for 0, 10, 22, 34, and 46 ms, as labeled. Holding potential was −35 mV. (C) Model traces were computed by first fitting experimental records during steps from −35 to −150 and −110 mV (as in Fig. 6), and then running −150/−110-mV two-step computations with the same prehyperpolarization durations as in experimental records (traces not labeled for clarity). Values of parameters y4, z, τ4L, and τK used to fit traces were as follows: 0.9998, 0.99, 0.0919, and 0.01 s at −150 mV; and 0.9819, 0.98, 0.491, and 0.08 s at −110 mV, respectively. (B and D) Semilog plots of experimental (B) and theoretical traces (D) at −110 mV corresponding to 0, 22, and 46 ms prehyperpolarizing steps to −150 mV (as labeled in B). In all plots, currents are referred to their steady-state level (630 pA).

−150 mV accelerated activation at −110 mV and progressively removed the delay until monoexponential time course was achieved with a 22-ms prepulse (see also semilog plots in Fig. 8 B) monoexponential time course was achieved.

To verify the ability of the allosteric model to mimic this behavior, we fitted records at −110 mV and at −150 mV with the procedure used above (Fig. 6), and then ran two-step model computations reproducing experimental protocols (Fig. 8 C). The model accurately predicted a progressive current acceleration and removal of delay with increasing prepulse durations. With sufficiently long prepulses, the computed time course became a single exponential, as apparent from the semilog plot of Fig. 8 D. This is expected if the action of prehyperpolarizing steps is to "prime" the channel opening process by pushing the majority of voltage sensors to their willing state, such that at −110 mV, the current development reflects mostly C4→O4 transitions. The computed traces at −110 mV, however, did not perfectly overlap experimental ones particularly after the longest prepulses. This may be due to the fact that, especially with long prepulses, the experimental current at −110 mV underwent an early acceleration compared with a single exponential (also observed in native f-channel; DiFrancesco and Ferroni, 1983; DiFrancesco, 1984), as evident in the semilog plots of Fig. 8 D (46-ms prepulse record). The model constraints do not allow to reproduce this behavior.

DISCUSSION

Early investigation of native pacemaker f-channels has shown that description of detailed kinetic properties requires a complex multistate, non-HH model (DiFrancesco, 1984). Experimental evidence presented here indicates that some features of the voltage-dependent gating of various HCN channel isoforms (mHCN1, hHCN2, and hHCN4) also do not comply with HH kinetics. These features include the following: (1) sigmoidal activation that cannot be approximated by the nth

power of an exponential; (2) sigmoidal deactivation; and (3) removal of the activation delay by prehyperpolarizing steps. This indicates that a multistate non-HH kinetic model may be required for HCN channels.

HCN channels belong to the superfamily of Kv and CNG channels. The amino acid sequence comprises six transmembrane (TM) domains with a pore region between S5 and S6 and a positively charged domain S4, which acts as the primary voltage sensor (Vaca et al., 2000; Chen et al., 2000). The structural similarities to 6-TM domain channels favor the hypothesis that HCN channel subunits coassemble as tetramers, and that their voltage-dependent closed/open transitions are governed by the voltage sensitivity of S4 movement.

A gating model taking into account the molecular information available and the structural similarities with Kv and CNG channels should, therefore, regard HCN channels as tetramers whose closed/open transitions are regulated by voltage sensors. Two additional observations help clarify the features of this model: first, previous work on native f-channels has shown that the cAMP-induced modulation can be described by an allosteric model (DiFrancesco, 1999); second, allosteric voltage-dependent gating has been proposed for other channels, including Ca^{2+} channels (Marks and Jones, 1992), *Shaker* K^+ channel (McCormack et al., 1994), and large conductance, Ca^{2+}-activated (*mSlo*) K^+ channels (Horrigan and Aldrich, 1999; Horrigan et al., 1999).

Allosteric Model of HCN Channels Voltage Gating and Comparison with Previous Models

Based on the above considerations, we asked whether the voltage gating of HCN channels could be described as an allosteric process, which led to a 10-state cyclic reaction scheme (Fig. 2). A major problem that we faced in using the model was to restrict the choice of free model parameters in a way that would allow the selection of parameter values by data fitting, since clearly too many free parameters would imply the need of arbitrary selection of some of the values.

One assumption of the model at one time intuitive and useful to the effect of limiting free parameters, was to consider that the action on closed/open channel ratio of any voltage sensor's displacement is always the same, regardless of the distribution of voltage sensors (i.e., the number of sensors in the willing state versus those in the reluctant state), or to which channel subunit the voltage sensor belongs. This meant that the parameter a could be considered as a constant (in the range 0–1). This assumption, together with the assumption of balanced rate constant changes (i.e., when the equilibrium constant is multiplied by a, then the opening rate constant is divided by $\sqrt{a}$, and the closing rate constant is multiplied by $\sqrt{a}$), was very effective in that it reduced the set of 10 originally free "vertical" rate constants in Fig. 2 (α, β, $\alpha1$, $\beta1$, $\alpha2$, $\beta2$, $\alpha3$, $\beta3$, $\alpha4$, and $\beta4$) to just three free rate constants (the parameter a and α, β or, equivalently, $\alpha4$ and $\beta4$).

On this basis, after a preliminary selection of model parameters (Table I), we used individual curve fitting to estimate rate constants (Figs. 4–6 and Table II). In all three HCN isoforms investigated, the allosteric scheme of Fig. 2 could reproduce the observed kinetic behavior, including sigmoidal activation and deactivation (Figs. 4–6) and removal of activation delay by prehyperpolarizations (Fig. 8). Also, the model accounted for the position and shape of the open probability curve for the three isoforms (Fig. 7).

The allosteric scheme examined here is analogous to that proposed by Marks and Jones (1992) for dihydropyridine-sensitive Ca^{2+} channels, by Rìos et al. (1993) for the Ca^{2+}-release channel of sarcoplasmic reticulum of skeletal muscle, by McCormack et al. (1994) for *Shaker* K^+ channels, and by Aldrich and collaborators for large conductance Ca^{2+}-activated K^+ (*mSlo*) channels (Horrigan and Aldrich, 1999; Horrigan et al., 1999). A distinct property of *mSlo* channels is the presence of a region of shallow slope in the time constant curve at high negative voltages; according to the allosteric hypothesis, this can be interpreted as due to a weak voltage dependence of closed/open transitions, which are slower than voltage sensor transitions and rate-limiting at large negative voltages (Horrigan et al., 1999).

In our model of HCN channels, closed/open transitions are indeed severalfold slower than sensor transitions for all isoforms (see Fig. 10); however, fitting of the time constant curves in Fig. 3 A and curve reconstruction in Figs. 4–6 indicate that closed/open transitions have a substantial voltage dependence ($z_\beta = -z_\alpha = 0.94$, 1.07, and 0.80 equivalent electronic charges for HCN1, HCN2, and HCN4 isoform, respectively, Table II).

It is important to stress that the values of z_α and z_β reported in Table II were not assumed, but resulted from data fitting, and, therefore, cannot be reduced arbitrarily. In other words, the assumption that each voltage sensor contributes equally to favor channel opening, together with the other model assumptions, leads to experimental data fitting indicating the presence of a substantial voltage dependence for closed/open transitions for all isoforms.

Investigating a model where closed/open transitions are weakly voltage-dependent would imply a different set of assumptions, since most of the voltage dependence of kinetics would derive from voltage sensors' state changes. The operating framework of the model would be likely to change significantly. We would need to release the assumptions concerning the constancy of a and/or the balanced rate constant changes, and let most of the 10 vertical rate constants α, β, $\alpha1$, $\beta1$, $\alpha2$, $\beta2$, $\alpha3$, $\beta3$, $\alpha4$, and $\beta4$

free to vary. In fact, the situation could be even more complex since releasing the condition a = constant would also affect the horizontal rate constants.

We did not adopt this solution because it would have involved too much arbitrariness in the selection of parameter values. More importantly, we did not have any real indication that closed/open transitions are weakly voltage-dependent or voltage-independent for HCN channels, since we did not have evidence for regions of shallow slope at negative voltages in time constant curves of any of the HCN isoforms investigated (Fig. 3 A). However, the model scheme of Fig. 2 is not incompatible with a situation where closed/open transitions are nearly voltage-independent (i.e., with a low z_α) and most of the voltage dependence of channel kinetics is attributable to sensor movements. Although we lack experimental evidence, we cannot rule out this possibility entirely, since, due to experimental constraints, the voltage range where recordings could be made was limited (positive to −135 mV; Fig. 3 A).

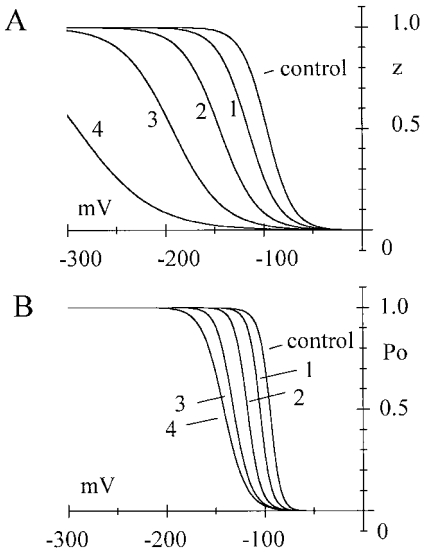

FIGURE 9. Allosteric model prediction of Po dependence on equivalent charge number of voltage sensor transitions. Calculations were performed for HCN2 channels using the parameters in Table II. (A) Willing/reluctant distribution parameter (z) calculated with Eqs. A9 and A10 in reference conditions (control) and after reduction of the equivalent charge number (z_δ = 1.021) by 1/6, 2/6, 3/6, and 4/6 (1–4). This was meant to mimic replacement of one to four basic residues with neutral ones in the simplified assumption that each residue contributes the same charge and that only six of the nine basic residues of S4 sense voltage changes. The latter hypothesis is based on the consideration that since S4 of HCN2 extends for 28 amino acids, more than the length of a membrane spanning α-helix (~20 amino acids), only a fraction of the full S4 length is likely to sense voltage changes (Chen et al., 2000). The slope of the distribution curve at midpoint voltages decreases in proportion to z_δ. (B) Po curves calculated by Eqs. A13 with A9 and A14 with the same z_δ values as in A, as indicated. The curve midpoint shifts to more negative voltages by 10.2, 22.9, 37, and 46.9 mV (1–4), whereas the slope decreases minimally with decreases of z_δ.

Implications of Allosteric Design

Recent data have shown that replacement of basic residues in the S4 segment of HCN2 with neutral ones leads to negative shifts of the activation curve voltage dependence (Chen et al., 2000; Vaca et al., 2000). However, the slope of the activation curve did not decrease as expected if it were correlated to the total number of equivalent charges moving through the electric field during activation/deactivation. The allosteric model may provide a simple explanation for these results, as illustrated in the example of Fig. 9 for HCN2.

In Fig. 9 A, the sensor distribution parameter z (reluctant/willing configurations) was assumed to undergo changes due to reduction of the equivalent charge number (z_δ) by 1/6, 2/6, 3/6, and 4/6 of the control value (labeled 1–4). As expected, reductions of z_δ led to proportional reductions in the slope of the z(V) curve. However, in Fig. 9 B, the Po(V) relations calculated with the different z(V) curves in Fig. 9 A were shifted to more negative voltages (by up to 46.9 mV with a four-sixths reduction) with only a minor change in slope. Thus, a possible explanation for the lack of modification of the slope of the activation curve in experiments where charged residues are mutated is that the activation process can be separated, as in the allosteric model proposed here, into two distinct steps (i.e., redistribution of voltage sensors and closed/open transitions). A direct consequence is that the slope of the Po curve does not necessarily reflect the slope of gating charge voltage dependence. Since the model provides a molecular interpretation of gating properties of HCN channels, it will be interesting to use it to simulate expectations of experiments in which structural elements of HCN channels are modified (i.e., mutations and/or coexpression of different isoforms).

Model Interpretation of the Different Kinetic Features of HCN Isoforms

The kinetics and cAMP dependence of different HCN isoforms differ quantitatively. For example, HCN1 subunits form channels with fast voltage-dependent gating and reduced cAMP sensitivity, whereas HCN2 and HCN4 channels respond more efficiently to cAMP and have slower kinetics (Santoro et al., 1998; Seifert et al., 1999; Ishii et al., 1999; Ludwig et al., 1999; this work). The allosteric scheme proposed accounts for quantitative differences in gating properties among HCN isoforms within the framework of a common reaction model. To help understand how the different kinetic properties of HCN isoforms can be interpreted according to the allosteric scheme, we superimposed in Fig. 10 plots of the rate parameters obtained for the three iso-

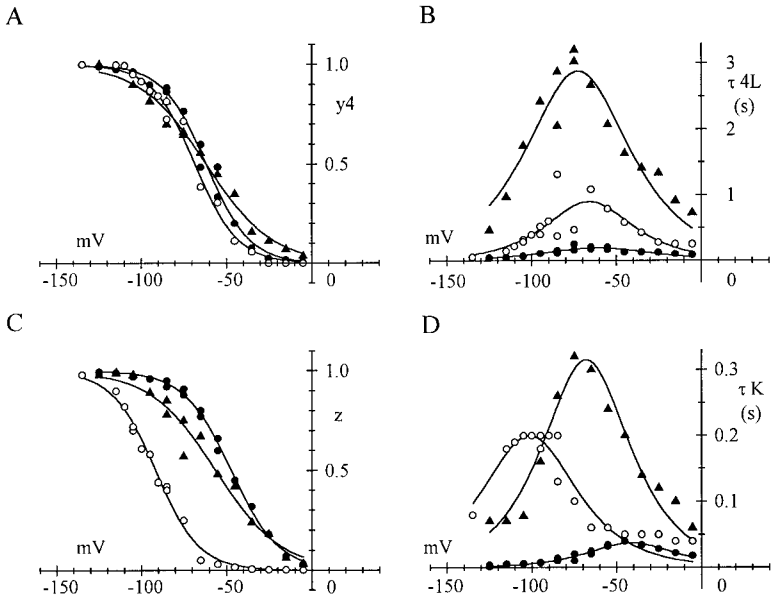

FIGURE 10. Comparison of allosteric gating parameters among HCN isoforms. In the plots the parameters y4 (A), τ4L (B), z (C,) and τK (D) determined by fitting kinetic data in Figs. 4–6 are superimposed along with their best-fitting curves (lines) for the isoforms HCN1 (closed circles), HCN2 (open circles), and HCN4 (closed triangles).

forms investigated by the fitting procedures in Figs. 4–6 ([closed circles] HCN1; [open circles] HCN2; [closed triangles] HCN4) along with their best-fitting curves. These plots are representative of both kinetic and steady-state channel properties according to the allosteric model (see superimposition of Po values in Fig. 7).

The comparison led to the following observations: (1) the y4(V) curves of all three isoforms are almost superimposable; (2) the voltage dependence of τ4L(V) curves is similar for all isoforms, the main difference being a scaling-up factor when going from HCN1 to HCN2 and HCN4 curves; (3) the z(V) curves of HCN1 and HCN4 are little different, whereas that of HCN2 is some 40 mV more negative; and (4) a similarly large voltage shift is present for the τK(V) curve of HCN2 relative to HCN1 and HCN4 curves; the peak τK increases when going from HCN1 to HCN2 and to HCN4.

The above observations allow a few tentative speculations on the mechanisms responsible for the kinetics of HCN channels and their differences. First, a scaling-up of time constant curve that leaves unaltered the distribution curve implies in a Boltzmann mechanism that on- and off-rates are divided by the same factor (>1), equivalent to adding a fixed positive energy term to the energy changes associated to on- and off-reactions. The data in Fig. 10 (A and B), thus, would be compatible with the assumption that closed/open transitions of HCN channels involve two mechanisms: (1) a voltage-dependent one, similar for all isoforms and involving movement of an equivalent electric charge of ~1; and (2) a voltage-independent "mechanical" one perhaps associated to intersubunit interactions that are loose in HCN1, tighter in HCN2, and tighter still in HCN4 channels. Assuming simple scaling-up of time constant curves, the τ4L curve of HCN1 is ~5 and 15 times smaller than those of HCN2 and HCN4, respectively. Compared with HCN1, the extra energies required by HCN2 and HCN4 closed/open transitions, thus, would be RT ln(5) = 0.956 kcal/mol and RT ln(15) = 1.609 kcal/mol (see Eqs. A9 and A10).

Second, according to the data in Fig. 10, faster activation of HCN1 relative to HCN2 and HCN4 is attributable to both faster voltage sensor activation and channel opening, whereas the more negative position of the HCN2 activation curve relative to that of HCN1 or HCN4 (Fig. 7) essentially depends on the voltage dependence of voltage sensors. Third, transition rates of voltage sensors are several times faster than closed/open transition rates, implying that for all isoforms, the activation process involves early sensor movements (from reluctant to willing states) as a preliminary requirement for efficient channel opening. Finally, lack of major changes in the equivalent charge associated to movement of voltage sensors and closed/open transitions suggests common structural rearrangements responsible for voltage-dependent state changes in the isoforms studied.

APPENDIX

Kinetics of Allosteric Model

A general set of equations governing the kinetics of the scheme in Fig. 2 is

$$\frac{dp_i}{dt} = -\left(\sum_{j \neq i} k_{i,j}\right)p_i + \sum_{j \neq i}(k_{j,i}p_j) \qquad i = 1,2\ldots n \quad (A1)$$

where p_i is the probability of state i, $k_{i,j}$ is the rate constant for the transition i to j, and n is the number of possible states (DiFrancesco, 1984). The system can be reduced by one degree by use of the relation $\Sigma p_i = 1$ and expressed in matrix notation as

$$\frac{dp}{dt} = A \cdot p + k, \quad (A2)$$

where the vectors p and k and the matrix A are defined as:

$$p = [p_1, p_2 \ldots p_{n-1}], \tag{A3}$$

$$k = [k_{n,1}, k_{n,2} \ldots k_{n,n-1}], \tag{A4}$$

To apply the general Eqs. A1–A5 to the scheme of Fig. 2, it is useful to first define the rate constants $k_{i,j}$. As illustrated in the legend to Fig. 2, the following relations hold for equilibrium constants and rate constants in the reaction scheme (note that $a = 1/f^2$):

$$K = \frac{4[C]}{[C1]} = \frac{3[C1]}{2[C2]} = \frac{2[C2]}{3[C3]} = \frac{[C3]}{4[C4]} = \frac{\delta}{\gamma};$$

$$aK = \frac{\delta/f}{\gamma f} = \frac{K}{f^2}$$

$$L = \frac{[C]}{[O]} = \frac{\beta}{\alpha}; \qquad Li = \frac{[Ci]}{[Oi]} = \frac{\beta i}{\alpha i} = a^i L \quad (i = 1\text{–}4)$$

$$\alpha i = \alpha f^i; \qquad \beta i = \frac{\beta i}{f^i} \qquad (i = 1\text{–}4) \tag{A6}$$

Using the numbering of states 1–10 as labeled in Fig. 2 and the relations A6, the rate constants $k_{i,j}$ can be tabulated as in Table A1.

We can now explicitly write the elements of Eq. A2 as follows:

$$p = [p_1, p_2, p_3, p_4, p_5, p_6, p_7, p_8, p_9] \tag{A7a}$$

$$k = \left[0,0,0,0,\frac{\beta}{f^4},0,0,0,\frac{4\delta}{f}\right] \tag{A7b}$$

Although integration of Eq. A2 is possible (Di-Francesco, 1984), the complexity of the system makes an analytical solution too difficult and requires numerical integration. The system is fully described once the parameter f (or $a = 1/f^2$) and the rate constants α, β, γ and δ are known. The voltage dependence of rate constants can be described by Boltzmann functions:

$$\begin{aligned} \alpha(V) &= \alpha o \exp(z_\alpha V/r) \\ \beta(V) &= \beta o \exp(z_\beta V/r) \\ \gamma(V) &= \gamma o \exp(z_\gamma V/r) \\ \delta(V) &= \delta o \exp(z_\delta V/r), \end{aligned} \tag{A9}$$

TABLE A1

Rate Constants $k_{i,j}$ for the Reaction Scheme of Fig. 2

	j = 1	2	3	4	5	6	7	8	9	10
i = 1		4γ				α				
2	δ		3γ				αf			
3		2γ		2γ				αf^2		
4			3δ		γ				$\alpha f 3^2$	
5				4δ						αf^4
6	β						$4\gamma f$			
7		β/f^2				δ/f		$3\gamma f$		
8							$2\delta/f$		$2\gamma f$	
9			β/f^3					$3\delta/f$		γf
10				β/f^4					$4\delta/f$	

where αo, βo, γo, and δo are rate constants at zero voltage, z_α, z_β, z_γ, and z_δ are the equivalent units of electronic charge moving in the electric field during corresponding state transitions, and $r = RT/F = 25.85$ mV ($T = 300°K$). It is assumed that $z_\beta = -z_\alpha$ and $z_\gamma = -z_\delta$. The former assumption is based on the experimental observation that activation and deactivation rate constants of native pacemaker channels have a nearly symmetrical dependence on voltage (Noble et al., 1989; Di-Francesco, 1999); the latter considers that the charge moved across the electric field upon transition of a voltage sensor from a reluctant to a willing state is equal and opposite to that moved in the reverse reaction. Numerical description of the kinetics of Fig. 2 scheme, thus, depends on knowledge of the six parameters αo, βo, γo, δo, z_β, and z_δ and of the parameter a.

An equivalent description, useful to a more intuitive interpretation of the meaning of parameters, can be obtained by using fractional distribution parameters and time constants. One such set of parameters equivalent to Eq. A9 is for example:

$$\begin{aligned} y4(V) = 1/(1 + L4) &= 1/(1 + \beta 4/\alpha 4); \\ \tau 4L(V) &= 1/(\alpha 4 + \beta 4) \\ z(V) = 1/(1 + K) &= 1/(1 + \delta/\gamma); \\ \tau K(V) &= 1/(\gamma + \delta). \end{aligned} \tag{A10}$$

$$A = \begin{bmatrix} -\left(\sum_{j \neq i} k_{i,j}\right) - k_{n,1} & k_{2,1} - k_{n,1} & k_{3,1} - k_{n,1} & \cdots & k_{n-1,1} - k_{n,1} \\ k_{1,2} - k_{n,2} & -\left(\sum_{j \neq 2} k_{2,j}\right) - k_{n,2} & k_{3,2} - k_{n,2} & \cdots & k_{n-1,2} - k_{n,2} \\ \cdots & \cdots & \cdots & \cdots & \cdots \\ k_{1,n-1} - k_{n,n-1} & k_{2,n-1} - k_{n,n-1} & k_{3,n-1} - k_{n,n-1} & \cdots & -\left(\sum_{j \neq n-1} k_{n-1,j}\right) - k_{n,n-1} \end{bmatrix} \tag{A5}$$

$$A = \begin{bmatrix}
-4\gamma-\alpha & \delta & & & & \beta & & & \\
4\gamma & \begin{matrix}-\delta-\alpha 1\\ -3\gamma\end{matrix} & 2\gamma & & & & \beta 1 & & \\
 & 3\gamma & \begin{matrix}-2\delta-\alpha 2\\ -2\gamma\end{matrix} & 3\delta & & & & \beta 2 & \\
 & & 2\gamma & \begin{matrix}-3\delta-\alpha 3\\ -\gamma\end{matrix} & 4\delta & & & & \beta 3 \\
-\beta 4 & -\beta 4 & -\beta 4 & \gamma-\beta 4 & \begin{matrix}-4\delta-\alpha 4\\ -\beta 4\end{matrix} & -\beta 4 & -\beta 4 & -\beta 4 & -\beta 4 \\
\alpha & & & & & -\beta-4\gamma f & \delta/f & & \\
 & \alpha 1 & & & & 4\gamma f & \begin{matrix}-\delta/f-\beta 1\\ -3\gamma f\end{matrix} & 2\delta/f & \\
 & & \alpha 2 & & & & 3\gamma f & \begin{matrix}-2\delta/f\\ -\beta 2-2\gamma f\end{matrix} & 3\delta/f \\
-4\delta/f & -4\delta/f & -4\delta/f & \alpha 3-4\delta/f & -4\delta/f & -4\delta/f & -4\delta/f & 2\gamma f-4\delta/f & \begin{matrix}-3\delta/f-\beta 3-\gamma f\\ -4\delta/f\end{matrix}
\end{bmatrix} \tag{A8}$$

(note that $\alpha 4 = \alpha/a^2$ and $\beta 4 = \beta\, a^2$ according to A6). Here y4 and z represent the fractional distribution between channel states O4 and C4 and between sensor willing and reluctant states, and $\tau 4L$ and τK represent the corresponding time constants of equilibrium changes.

An explicit solution of A2 describing the probability of open state can be obtained by the MWC formulation of cyclic allosteric reactions (Monod et al., 1965). At equilibrium:

$$\begin{aligned}
&[O] = [C]\,(1/L)\\
&[O1] = [O]/(aK/4); \qquad [C1] = [C]/(K/4)\\
&[O2] = [O1]/(2aK/3); \qquad [C2] = [C1]/(2K/3)\\
&[O3] = [O2]/(3aK/2); \qquad [C3] = [C2]/(3K/2)\\
&[O4] = [O3]/(4aK); \qquad [O4] = [O3]/(4K)
\end{aligned} \tag{A11}$$

Summing over open and closed states and rearranging yields total open ([Ot]) and total closed ([Ct]) concentrations:

$$\begin{aligned}
[Ot] &= [O] + [O1] + [O2] + [O3] + [O4]\\
&= [O]\sum_{i=1}^{4}\binom{4}{i}\frac{1}{aK^i} = [O]\left(1+\frac{1}{aK}\right)^4\\
[Ct] &= [C] + [C1] + [C2] + [C3] + [C4]\\
&= [C]\sum_{i=1}^{4}\binom{4}{i}\frac{1}{K^i} = [C]\left(1+\frac{1}{K}\right)^4\\
&= L[O]\left(1+\frac{1}{K}\right)^4,
\end{aligned} \tag{A12}$$

from which the probability of open state is derived as

$$Po = \frac{[Ot]}{[Ot]+[Ct]} = \frac{1}{1+L\left(\frac{1+1/K}{1+1/aK}\right)^4}. \tag{A13}$$

The voltage dependence of Po results from the voltage dependence of rate constants according to Eq. A9 and the definition of equilibrium constants L and K in the scheme of Fig. 2:

$$\begin{aligned}
L(V) &= \beta(V)/\alpha(V) = (\beta o/\alpha o)\exp((z_\beta - z_\alpha)V/r)\\
&= \exp((2z_\beta)((V-VL)/r))\\
K(V) &= \delta(V)/\gamma(V) = (\delta o/\gamma o)\exp((z_\delta - z_\gamma)V/r)\\
&= \exp((2z_\delta)((V-VK)/r)),
\end{aligned} \tag{A14}$$

where

$$\begin{aligned}
VL &= -(r/(2z_\beta))\ln(\beta o/\alpha o)\\
VK &= -(r/(2z_\delta))\ln(\delta o/\gamma o)
\end{aligned} \tag{A15}$$

are the midpoint voltages of the fractional distribution parameters $y = 1/(1+L)$ (distribution between O/C states) and $z = 1/(1+K)$ (distribution between willing/reluctant sensor states). As mentioned above (Eq. A10) an equivalent description can be obtained by referring to C4↔O4, rather than C↔O transitions. In this case, the variables used are (see Eq. A6):

$$\begin{aligned}
L4(V) &= \beta 4(V)/\alpha 4(V) = a^4\beta(V)/\alpha(V)\\
&= (a^4 L4(V) = \exp((2z_\beta)((V-V4L/r)))
\end{aligned} \tag{A16}$$

$$V4L = -(r/(2z_\beta))\ln(\beta 4o/\alpha 4o)$$
$$= -(r/(2z_\beta))\ln[a^4(\beta o/\alpha o)] \quad \text{(A17)}$$
$$= VL - (2r\ln(a)/z_\beta)$$

and from A13

$$Po = \frac{1}{1 + L4\left(\frac{1+K}{1+aK}\right)^4}. \quad \text{(A18)}$$

We thank Antonio Malgaroli, Richard B. Robinson and Arnaldo Ferroni for discussion, and Monica Beltrame for assistance in development of the molecular biology of HCN clones. We also wish to thank B. Santoro and S. Siegelbaum (Columbia University, New York, NY) for supplying mHCN1 cDNA, and U.B. Kaupp of the University of Jülich for supplying hHCN4 cDNA.

This work was supported by the MURST (Cofin 1999 to D. DiFrancesco) and by Telethon (Grant no 971 to D. DiFrancesco).

Submitted: 19 December 2000
Revised: 9 April 2001
Accepted: 13 April 2001

REFERENCES

Chen, J., J.S. Mitcheson, M. Lin, and M.C. Sanguinetti. 2000. Functional role of charged residues in the putative voltage sensor of the HCN2 pacemaker channel. *J. Biol. Chem.* 275:36465–36471.

Clapham, D.E. 1998. Not so funny anymore: pacing channels are cloned. *Neuron.* 21:1–5.

DiFrancesco, D. 1984. Characterization of the pacemaker current kinetics in calf Purkinje fibres. *J. Physiol.* 348:341–367.

DiFrancesco, D. 1985. The cardiac hyperpolarizing-activated current, i_f. Origins and developments. *Prog. Biophys. Mol. Biol.* 46:163–183.

DiFrancesco, D. 1993. Pacemaker mechanisms in cardiac tissue. *Annu. Rev. Physiol.* 55:455–472

DiFrancesco, D. 1999. Dual allosteric modulation of pacemaker (f) channels by cAMP and voltage in rabbit SA node. *J. Physiol.* 512: 367–376.

DiFrancesco, D., and A. Ferroni. 1983. Delayed activation of the cardiac pacemaker current and its dependence on conditioning pre-hyperpolarizations. *Pflügers Arch.* 396:265–267.

DiFrancesco, D., A. Ferroni, M. Mazzanti,. and C. Tromba. 1986. Properties of the hyperpolarizing-activated current (if) in cells isolated from the rabbit sino-atrial node. *J. Physiol.* 377:61–88.

Gauss, R., R. Seifert, and B.U. Kaupp. 1998. Molecular identification of a hyperpolarization-activated channel in sea urchin sperm. *Nature.* 393:583–587.

Horrigan, F.T., and R.W. Aldrich. 1999. Allosteric voltage gating of potassium channels II. Mslo channel gating charge movement in the absence of Ca^{2+}. *J. Gen. Physiol.* 1142:305–336.

Horrigan, F.T., J. Cui, and R.W. Aldrich. 1999. Allosteric voltage gating of potassium channels I. Mslo ionic currents in the absence of Ca^{2+}. *J. Gen. Physiol.* 1142:277–304.

Ishii, T.M., M. Takano, L.H. Xie, A. Noma, and H. Ohmori. 1999. Molecular characterization of the hyperpolarization-activated cation channel in rabbit heart sinoatrial node. *J. Biol. Chem.* 274: 12835–12839.

Jones, S.W. 1999. Commentary: a plausible model. *J. Gen. Physiol.* 114:271–275.

Kinsella, T.M., and G.P. Nolan. 1996. Episomal vector rapidly and stably produce high-titer recombinant retrovirus. *Hum. Gene Ther.* 7:1405–1413.

Ludwig, A., X. Zong, M. Jeglitsch, F. Hofmann, and M. Biel. 1998. A family of hyperpolarization-activated mammalian cation channels. *Nature.* 393:587–591.

Ludwig, A., X. Zong, J. Stieber, R. Hullin, F. Hofmann, and M. Biel. 1999. Two pacemaker channels from human heart with profoundly different activation kinetics. *EMBO J.* 189:2323–2329.

Marks, T.N., and S.W. Jones. 1992. Calcium currents in the A7r5 smooth muscle-derived cell line. An allosteric model for calcium channel activation and dihydropyridine agonist action. *J. Gen. Physiol.* 993:367–390.

McCormack, K., W.J. Joiner, and S.H. Heinemann. 1994. A characterization of the activating structural rearrangements in voltage-dependent Shaker K^+ channels. *Neuron.* 122:301–315.

Monod, J., J. Wyman, and J.-P. Changeux. 1965. On the nature of allosteric transitions: a plausible model. *J. Mol. Biol.* 12:88–118.

Moroni A., A. Barbuti, C. Altomare, C. Viscomi, J. Morgan, M. Baruscotti, and D. DiFrancesco. 2000. Kinetic and ionic properties of human HCN2 pacemaker channels. *Pflügers Arch.* 439:618–626.

Noble, D., D. DiFrancesco, and J. Denyer. 1989. Ionic mechanisms in normal and abnormal cardiac pacemaker activity. *In* Neuronal and Cellular Oscillators. J.W. Jacklet, editor. Dekker, New York. 59–85.

Pape, H.C. 1996. Queer current and pacemaker: the hyperpolarization-activated cation current in neurons. *Annu. Rev. Physiol.* 58: 299–327.

Rìos, E., M. Karhanek, J. Ma, and A. Gonzalez. 1993. An allosteric model of the molecular interactions of excitation-contraction coupling in skeletal muscle. *J. Gen. Physiol.* 102:449–481.

Santoro, B., S.G. Grant, D. Bartsch,. and E.R. Kandel. 1997. Interactive cloning with the SH3 domain of N-src identifies a new brain specific ion channel protein, with homology to eag and cyclic nucleotide-gated channels. *Proc. Natl. Acad. Sci. USA.* 94:14815–14820.

Santoro, B., D.T. Liu, H. Yao, D. Bartsch, E.R. Kandel, S.A. Siegelbaum, and G.R. Tibbs. 1998. Identification of a gene encoding a hyperpolarization-activated pacemaker channel of brain. *Cell.* 935:717–729.

Seifert, R., A. Scholten, R. Gauss, A. Mincheva, P. Lichter, and U.B. Kaupp. 1999. Molecular characterization of a slowly gating human hyperpolarization-activated channel predominantly expressed in thalamus, heart, and testis. *Proc. Natl. Acad. Sci. USA.* 9616:9391–9396.

Vaca, L., J. Stieber, X. Zong, A. Ludwig, F. Hofmann, and M. Biel. 2000. Mutations in the S4 domain of a pacemaker channel alter its voltage dependence. *FEBS Lett.* 479:35-40.

Vaccari, T., A. Moroni, M. Rocchi, L. Gorza, M.E. Bianchi, M. Beltrame, and D. DiFrancesco. 1999. The human gene coding for HCN2, a pacemaker channel of the heart. *Biochim. Biophys. Acta.* 14463:419–425.